JCTC Journal of Chemical Theory and Computation

Theoretical Investigation of the Mechanism of Acid-Catalyzed Oxygenation of a Pd(II)-Hydride To Produce a Pd(II)-Hydroperoxide

Sugata Chowdhury, Ivan Rivalta, Nino Russo,* and Emilia Sicilia

Dipartimento di Chimica and Centro di Calcolo ad Alte Prestazioni per Elaborazioni Parallele e Distribuite-Centro d'Eccellenza MURST, Università della Calabria, I-87030 Arcavacata di Rende, Italy

Received April 29, 2008; Revised Manuscript Received June 6, 2008; Accepted June 9, 2008

Abstract: Density Functional Theory (DFT) has been applied to a comprehensive mechanistic study of the conversion reaction of the Pd(II)-hydride complex, $(IMe)_2(RCO_2)PdH$ (R=CH_3, Ph, and *p*-$O_2NC_6H_4$), to the corresponding Pd(II)-hydroperoxide in the presence of molecular oxygen. The calculations have evaluated the two mechanistic proposed alternatives, that are both considered viable on the basis of current data, of slow RCO_2H reductive elimination followed by oxygenation (*Path A*) and direct O_2 insertion (*Path B*). Results suggest that the mechanism of direct insertion of molecular oxygen into the Pd−H bond of the initial complex is energetically preferred. The activation energy relative to the rate-determining step of *Path A*, indeed, is calculated to be lower than the activation energy of the rate determining step of the alternative *Path B*, whatever ligand (CH_3CO_2, Ph, CO_2, *p*-$O_2NC_6H_4CO_2$) is coordinated to the Pd center. The calculated free activation energy of the rate-determining hydrogen abstraction step ($\Delta G^* =$ 24.8 kcal/mol) in the case of the oxygenation reaction of the benzoate-ligated Pd(II)-hydride complex is in very good agreement with the experimentally determined value of 24.4 kcal/mol. In addition, according to the experimentally detected enhancement of the reaction rate due to the presence of a nitro group on the benzoate ligand, our calculations show that the transition state for the hydrogen atom abstraction by molecular oxygen along the pathway for the oxygenation reaction of $(IMe)_2$(*p*-$O_2NC_6H_4CO_2$)PdH lies lower in energy with respect to the analogous transition state calculated for R=Ph.

1. Introduction

The use of molecular oxygen for the oxidative functionalization of organic molecules is a highly attractive option because O_2 is a readily available and nontoxic reagent. Additionally, a common byproduct of aerobic oxidations is the innocuous substance water. However, uncatalyzed chemical reactions between molecular oxygen and organic substrates generally result in complete combustion of the starting materials, and, consequently, the synthetic advantages these reactions possess cannot be exploited unless catalysts are used. The homogeneously Pd-catalyzed oxidations have emerged as a particularly promising reaction type for selective and efficient aerobic oxidation[1–7] even if the development of new and more efficient catalytic strategies has been hampered by an inadequate understanding of how O_2 interacts with the Pd center.[7] Two are the pathways proposed to explain how the oxygen activation in palladium-catalyzed oxidations proceeds (Scheme 1).

One pathway (*Path A*) is the formation of a Pd(0) species **II** through the reductive elimination of a HX species from the Pd(II)-hydride complex followed by the oxygenation of the Pd(0) center to form a η^2-peroxo Pd(II) species **III**. Upon protonation of the peroxopalladium(II) intermediate a pal-

* Corresponding author fax: +39-0984-492044; e-mail: nrusso@unical.it.

10.1021/ct8001442 CCC: $40.75
Published on Web 07/16/2008

Scheme 1

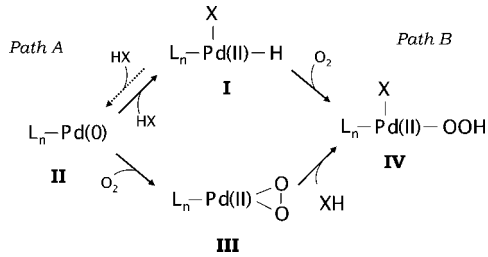

ladium hydroperoxide species **IV** is formed.[8–10] The second mechanistic possibility[11–13] (*Path B*) involves the direct insertion of molecular oxygen into a palladium(II)-hydride intermediate **I** to form the same palladium hydroperoxide species **IV** (Scheme 1) and, therefore, avoiding to proceed through Pd(0). The former mechanism has substantial experimental support even if the reaction between Pd(0) and triplet oxygen is spin forbidden.[8–10] Landis, Stahl, and co-workers have investigated this aspect performing a DFT theoretical study that showed the exothermic formation of the singlet Pd(II)-peroxido species requiring spin crossing between triplet and singlet surfaces mediated by spin−orbit coupling.[14]

The first observation of what can be assumed to be a direct insertion of molecular oxygen into a Pd(II)-hydride bond to form a hydroperoxopalladium complex has been reported by Goldberg, Kemp, and co-workers for a Pd complex that, due to the nature of the ligand, cannot undergo reductive elimination.[15] The authors report that benzene solutions of ($^{t\mathrm{Bu}}$PCP)PdH ($^{t\mathrm{Bu}}$PCP=1,3-$(CH_2P^tBu_2)_2C_6H_3]^-$) exposed to O_2 cleanly react to yield ($^{t\mathrm{Bu}}$PCP)PdOOH, which is relatively stable at ambient temperature as a solid and structurally characterizable. A DFT theoretical investigation, carried out by Goddard and co-workers, of the involved mechanism has recently appeared in literature that demonstrates how an insertion mechanism is possible and plausible and supports the hypothesis that the hydrogen atom abstraction is the key step of the reaction.[16] Namely, hydrogen atom is abstracted from the Pd center by molecular oxygen to form a HOO fragment that interacts only weakly with the Pd(I) center. Rotation of HO_2 moiety enables formation of a Pd−O bond to give the final Pd(II)-hydroperoxo product. A minimum energy crossing point (MECP) between triplet and singlet surfaces has been located at the exit channel of the reaction, whereas the mechanism for the rearrangement of the HOO fragment to give the hydroperoxide product has not been individuated. In the same work is discussed the difference with respect to a previous study of the same authors that underlined the subordination of the O_2 insertion process to the presence of a H-bond acceptor *cis* to the hydride.[17]

Stahl and co-workers have investigated the feasibility of the Pd(0) direct oxygenation pathway by subjecting [Pd(0)$(IMes)_2$] (IMes=Mesityl) to one equivalent of a carboxylic acid (acetic, benzoic, and *p*-nitrobenzoic) to produce the *trans*-[$(IMes)_2(RCO_2)$PdH] hydride, which subsequently exposed to O_2 yielded the corresponding hydroperoxide complex.[18] Since the experimental findings could support both mechanisms, that is direct insertion of O_2 into the Pd(II)-H bond and oxygenation of Pd(0), both pathways have been considered viable by the authors. Indeed, four possible alternative pathways have been computationally examined by Popp and Stahl to probe the reaction mechanism of the formal insertion of molecular oxygen into the Pd−H bond of *trans*-[PdH(OAc)$(IMes)_2$].[19] The main conclusion of this investigation is that the energetically preferred pathways, exhibiting very similar kinetic barriers, are those corresponding to (a) hydrogen atom abstraction from the Pd−H bond by molecular oxygen and (b) reductive elimination AcOH followed by oxygenation of Pd(0) and protonolysis of the formed η^2-peroxo-Pd(II) species. Also in this last case the proposed steps of the hydrogen abstraction mechanism are as follows: formation of a HOO moiety as a consequence of the hydrogen atom abstraction by molecular oxygen and formation of the final hydroperoxo product through rearrangement of the HO_2 fragment. In analogy with Goddard's analysis[16] the MECP between singlet and triplet PESs has been located at the exit channel of the reaction, but not one of the surmised mechanisms for the rearrangement of the HO_2 fragment has been confirmed.

In the framework of a more extended project aiming to unravel the mechanistic details of the selective oxidation of organic molecules by molecular oxygen in the presence of metal catalysts we have theoretically investigated the direct O_2 insertion mechanism for both ($^{t\mathrm{Bu}}$PCP)PdH and [$(IMes)_2$(AcO)PdH] hydrides.[20,21] With respect to the preceding computational analyses carried out on the same subject[16,19] the new results are as follows: the recognition of a different pathway for the process and the determination of the rearrangement mechanism of the OOH fragment as the last step of the overall hydride oxygenation reaction. In the present work we have examined the possible alternative mechanisms of the oxygenation process of the Pd-hydride complex *trans*-[Pd(H)$(O_2CR)(IMes)_2$] with R=CH_3, Ph, *p*-$O_2NC_6H_4$ to yield the corresponding hydroperoxide, taking into account also the influence on the oxygenation pathways of the employed carboxylic acid. Kinetic measurements,[18] indeed, have shown that the reaction rate exhibits a clear first-order dependence on the concentration of the Pd-hydride, and the presence of an electron-withdrawing nitro group on the benzoate ligand significantly enhances the reaction rate (when R=*p*-$O_2NC_6H_4$ the oxygenation is about eight times faster than when R=Ph). The ligand dependence could suggest that carboxylate dissociation is the rate determining step of the process and, as a consequence, supports the reaction mechanism involving reductive elimination of the carboxylic acid. Since many questions concerning the mechanistic details of the Pd-catalyzed oxidation reactions are still open,[22] the results of our computations can contribute to the determination of the true pathway for the interaction between molecular oxygen and Pd(II)-H complexes.

2. Computational Details

Geometry optimizations as well as frequency calculations for all the reactants, intermediates, products, and transition states have been performed at the Density Functional level of theory, employing the Becke's three-parameter hybrid functional[23] combined with the Lee, Yang, and Parr (LYP)[24] correlation functional, denoted as B3LYP, as implemented

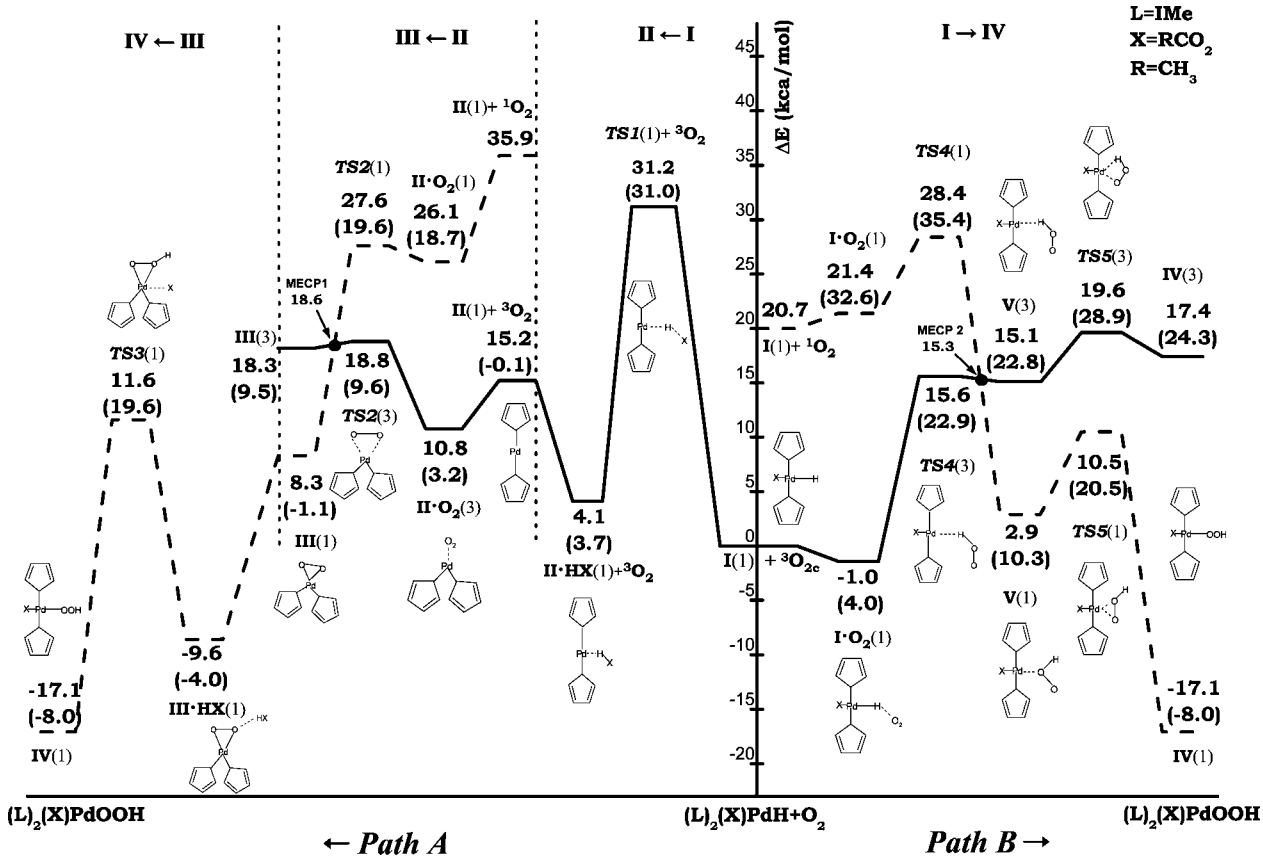

Figure 1. Calculated B3LYP PESs for the oxygenation reaction of $(IMe)_2(CH_3CO_2)Pd(II)$-H to give $(IMe)_2(CH_3CO_2)Pd(II)$-OOH. Gibbs free energies changes at 298.15 K in benzene are also reported in parentheses. Energies are in kcal/mol and relative to ground-state reactants. On the left the pathway that involves reductive elimination of CH_3COOH (*Path A*) and on the right the pathway for the direct O_2 insertion (*Path B*) are reported.

in Gaussian03 code.[25] For Pd the relativistic compact Stuttgart/Dresden effective core potential[26] has been used in conjunction with its split valence basis set. The 6−311G* basis sets of Pople and co-workers have been employed for the rest of the atoms. For each optimized stationary point vibrational analysis has been performed to determine its character (minimum or saddle point), and zero-point vibrational energy (ZPVE) corrections were included in all relative energies (ΔE). For transition states it was carefully checked that the vibrational mode associated with the imaginary frequency corresponded to the correct movement of involved atoms. Furthermore, the intrinsic reaction coordinate (IRC)[27,28] method has been used to assess that the localized TSs correctly connect to the corresponding minima along the imaginary mode of vibration.

To speed up calculations the 2,4,6-trimethylphenyl groups of the IMes ligands have been substituted with methyl ones to obtain a palladium hydride complex that, although less sterically hindered, can give analogous results.[19] For this reason, from now on we will indicate the 1,3-di(methyl)imidazoline-2-ylidene model of the ligand as IMe, and the starting points for our study are the *trans*[(RCO_2)(1,3-di(methyl)imidazoline-2-ylidene)$_2$PdH] species (R=CH_3, Ph, *p*-$O_2NC_6H_4$), also abbreviated as *trans*[$(RCO_2)(IMe)_2$PdH].

Both triplet and singlet reaction paths have been examined and for all the studied species $<S^2>$ values have been checked to assess whether spin contamination can influence the quality of the results. For triplet state structures no significant contamination was found by unrestricted calculations. Unrestricted calculations, instead, revealed in some cases triplet spin contamination corresponding to $<S^2>$ values close to 1.0. For molecular oxygen, due to the contamination of the singlet wave function with the triplet state, a highly stable singlet $^1\Delta_g$ state has been obtained corresponding to an excitation energy of 10.5 kcal/mol, compared with the experimental value of 22.5 kcal/mol.[29] Adopting the method proposed by Ovchinnikov and Labanowski[30] for correcting the mixed spin energies and removing the foreign spin components, a triplet-singlet energy gap of 20.7 kcal/mol was obtained, in very good agreement with the experimental value. The same scheme was adopted to correct the triplet contaminated energies of some structures along the singlet path, as will be underlined in the next paragraphs.

Solvent effects, both electrostatic and nonelectrostatic, have been treated implicitly making use of the Tomasi's integral equation formalism for the polarizable continuum model (IEF-PCM)[31,32] as implemented in Gaussian03. All stationary points structures obtained from vacuum calculations were reoptimized in implicit benzene with the above IEF-PCM method.

The solvation Gibbs free energies have been evaluated using the well-known thermodynamic cycle,[33] where the reaction Gibbs free energy in solution, ΔG_{sol}, is calculated for each process as the sum of two contributions: a gas-

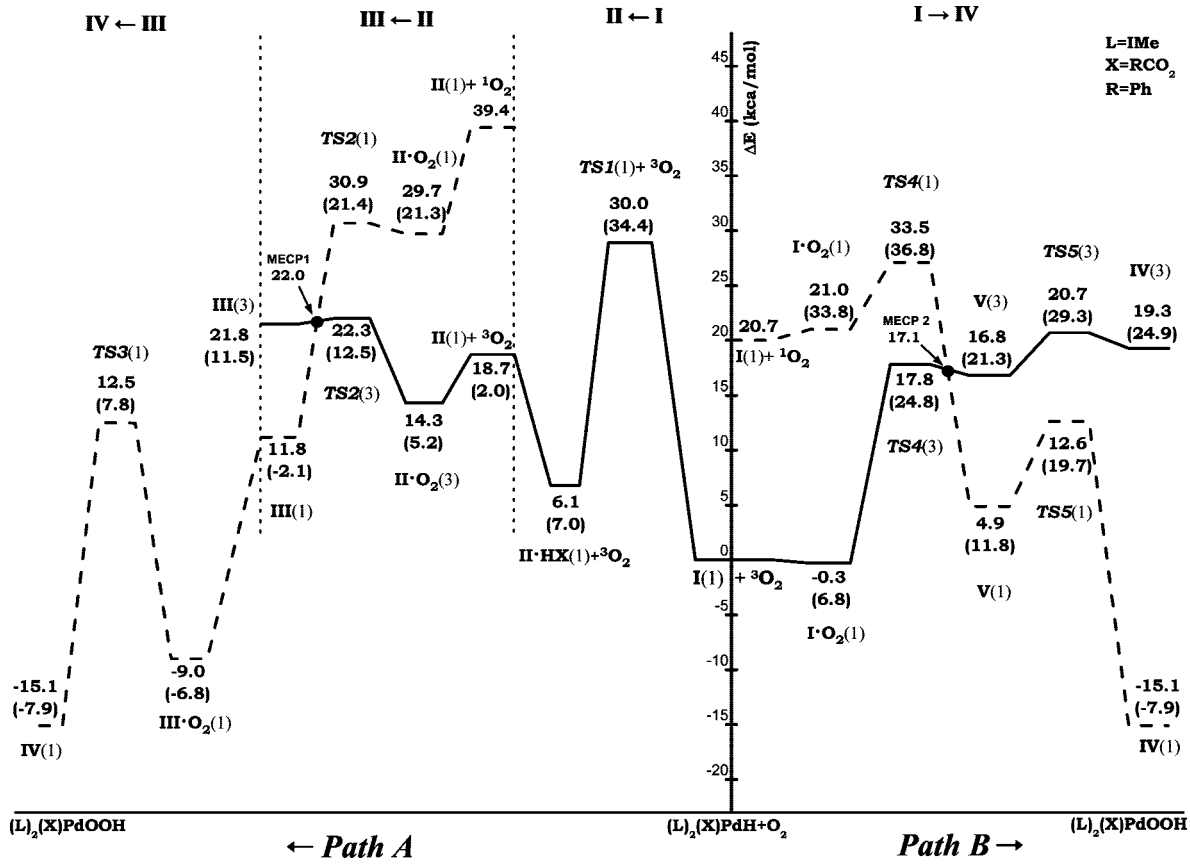

Figure 2. Calculated B3LYP PESs for the oxygenation reaction of $(IMe)_2(PhCO_2)Pd(II)$-H to give $(IMe)_2(PhCO_2)Pd(II)$-OOH. Gibbs free energies changes at 298.15 K in benzene are also reported in parentheses. Energies are in kcal/mol and relative to the ground-state reactants. On the left the pathway that involves reductive elimination of PhCOOH (*Path A*) and on the left the pathway for the direct O_2 insertion (*Path B*) are reported.

phase reaction free energy, ΔG_{gas}, and a solvation reaction free energy term calculated with the continuum approach, ΔG_{solv}:

$$\Delta G_{sol} = \Delta G_{gas} + \Delta G_{solv} \quad (1)$$

The gas-phase reaction free energy is the sum of two parts: electronic plus nuclear repulsion energy (ΔE_{ele}) and thermal contribution including zero-point energy ($\Delta G_{gas} = \Delta H + T\Delta S$). The last term, $T\Delta S$, that is the thermal correction, is evaluated using the calculated quantum mechanical vibrational frequencies.

To locate the minimum energy crossing points (MECP) between the triplet surfaces of reactants and the singlet ones of the products the methodology introduced by Harvey and co-workers has been used.[34]

3. Results and Discussion

Calculated B3LYP PESs for the oxygenation process of $(RCO_2)(IMe)_2PdH$ hydrides are drawn in Figures 1–3 for R=CH_3, Ph, *p*-$O_2NC_6H_4$, respectively. Both singlet and triplet PESs have been computed. Relative energies are calculated with respect to the ground-state reactants asymptote (**I**(1)+$^3O_2$). The energy profile for the steps of the pathway that, starting from the hydride species **I**, involves reductive elimination of RCOOH (R=CH_3, Ph, *p*-$O_2NC_6H_4$) to yield Pd(0) complex (**II**), oxygenation of **II** to yield the peroxo complex **III**, and subsequent protonation to form the hydroperoxide complex **IV** are shown on the left side of each figure (*Path A*). The calculated PESs for the direct insertion of O_2 into the Pd−H bond of the hydride species to obtain the same hydroperoxides are drawn on the right side of each figure (*Path B*). Relative free energies calculated in benzene solvent are also reported in Figures 1–3.

The ground-state optimized structure of the reference hydride species chosen as the starting point for our study is shown in Figure 4 along with the optimized structure of the final hydroperoxide complex in the case of R=Ph. Ground-state geometrical structures of all stationary points intercepted along the pathway for the $(PhCO_2)(IMe)_2PdH$ hydride oxygenation through reductive elimination, Pd(0) oxygenation, and protonolysis of peroxo complex are reported in Figure 5, whereas ground-state optimized structures of the sequence of minima and transition states involved by the direct O_2 insertion pathway are shown in Figure 6. In Figures 5 and 6 are sketched also the structures of the calculated MECPs. Labels employed in Figures 4–6 to individuate geometrical parameters have to be used to read information reported in Table 1 for *Path A* and Table 2 for *Path B*, which collect selected bond lengths and angles along with dihedral angles of stationary points and MECPs for R=CH_3, Ph, and *p*-$O_2NC_6H_4$.

In the next two paragraphs we are going to illustrate the outcomes of our calculations for both *Path A* and *Path B* in the case of R=CH_3. Subsequently, the results of our DFT

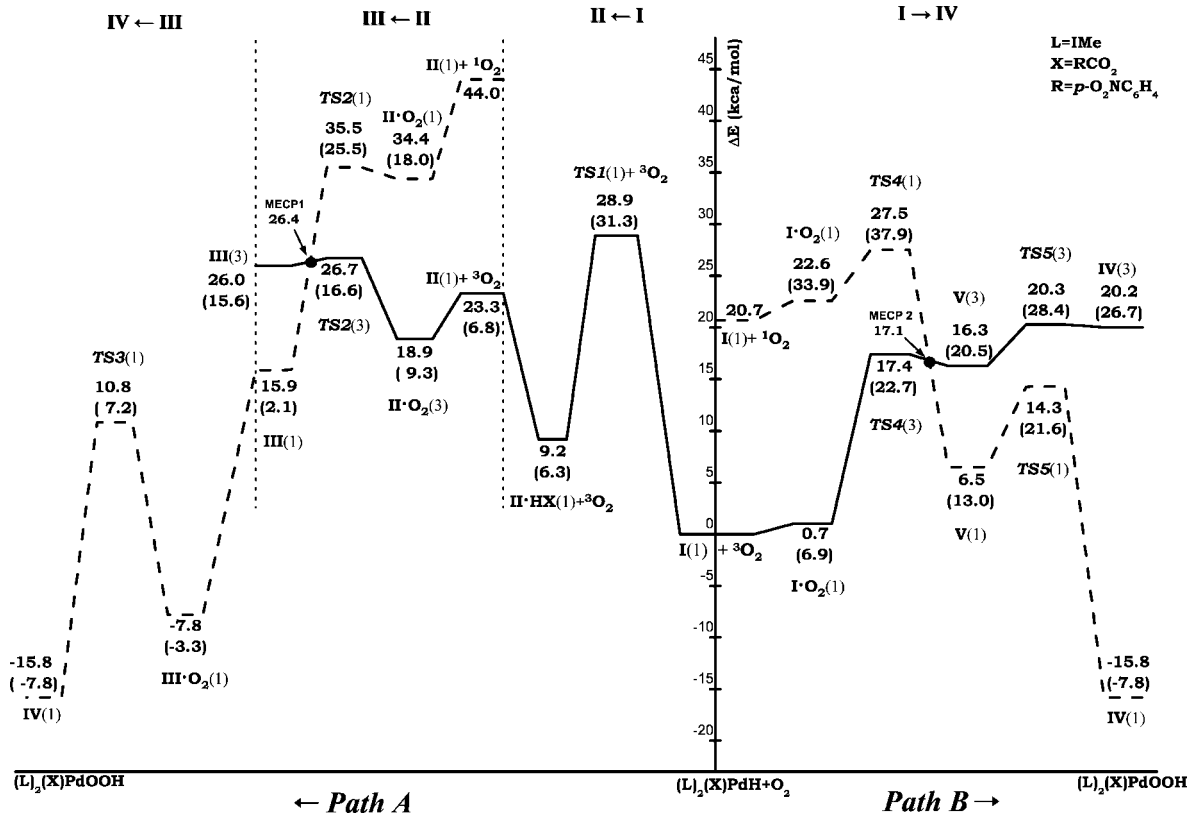

Figure 3. Calculated B3LYP PESs for the oxygenation reaction of $(IMe)_2(p\text{-}O_2NC_6H_5CO_2)Pd(II)\text{-}H$ to give $(IMe)_2(p\text{-}O_2NC_6H_5CO_2)Pd(II)\text{-}OOH$. Gibbs free energies changes at 298.15 K in benzene are also reported in parentheses. Energies are in kcal/mol and relative to the ground-state reactants. On the left the pathway that involves reductive elimination of $p\text{-}O_2NC_6H_5COOH$ (*Path A*) and on the right the pathway for the direct O_2 insertion (*Path B*) are reported.

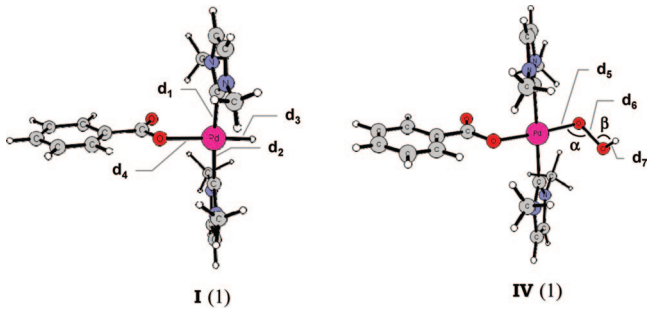

Figure 4. Ground-state optimized structures of the Pd(II)-H and Pd(II)-OOH complexes in the case of R=Ph. Labels employed to individuate geometrical parameters have to be used to read information reported in Tables 1 and 2.

analysis for R=Ph, $p\text{-}O_2NC_6H_4$ will be pointed out for comparison, and general conclusions on the viability of the alternative proposed mechanisms will be drawn.

3.1. Mechanism Proceeding via the Pd(0) Intermediate. The first step of the mechanism that involves formation of the Pd(0) species proceeds by reductive elimination of CH_3COOH from the initial Pd-hydride complex (Step **I** → **II**). As shown in Figure 1 the transition state **TS1***(1)*, which the reaction evolves through is very high in energy, with a calculated relative energy of about 31 kcal/mol both in gas phase and in solution. An inspection of Figure 1 clearly shows that this is the rate-determining step of the overall transformation. The calculated imaginary frequency is 485*i* cm^{-1} and is mainly associated with the displacement of the hydrogen atom from palladium to carbon atom. In the next minimum intercepted along the PES, **II·HX**(1), the carboxylic acid molecule still interacts with the Pd(0) formed species, and the process results to be endothermic by 4.7 kcal/mol (4.1 kcal/mol in gas phase). Formation of final products, upon reductive elimination of CH_3COOH from the initial Pd−H complex, is practically thermoneutral in solvent and endothermic by 15.2 kcal/mol in gas phase. The reaction between the formed Pd(0) complex with triplet molecular oxygen (Step **II**→**III**) requires that both singlet and triplet multiplicities are examined and leads initially to the formation of an η^1-O_2 adduct, **II·**O_2, in which the IMe ligands retain their *trans* configuration. A stable closed-shell singlet complex, **III**, is formed by surpassing a low energy barrier (6.4 kcal/mol in solvent and 10 kcal/mol in gas phase) corresponding to the transition state, **TS2**(3), for the IMe ligands *trans* to *cis* isomerization. The characteristics of this adduct **III** (O−O distance of 1.4 Å and O−O stretching frequency of 978 cm^{-1}) allow us to design it as a η^2-peroxide.[35] Due to the multiplicity change, in this region of the PES the system must undergo a spin inversion that takes place after passage of the **TS2** transition state. In the framework of the Two-State Reactivity paradigm[36] such a kind of spin crossover is not considered a rate-limiting factor as it involves species that are formed with excess energy, and even electronically excited states become accessible. Following the procedure outlined before, the MECP between the triplet and singlet surfaces has been individuated, and the structure at this point, **MECP1**, exhibits a geometry very

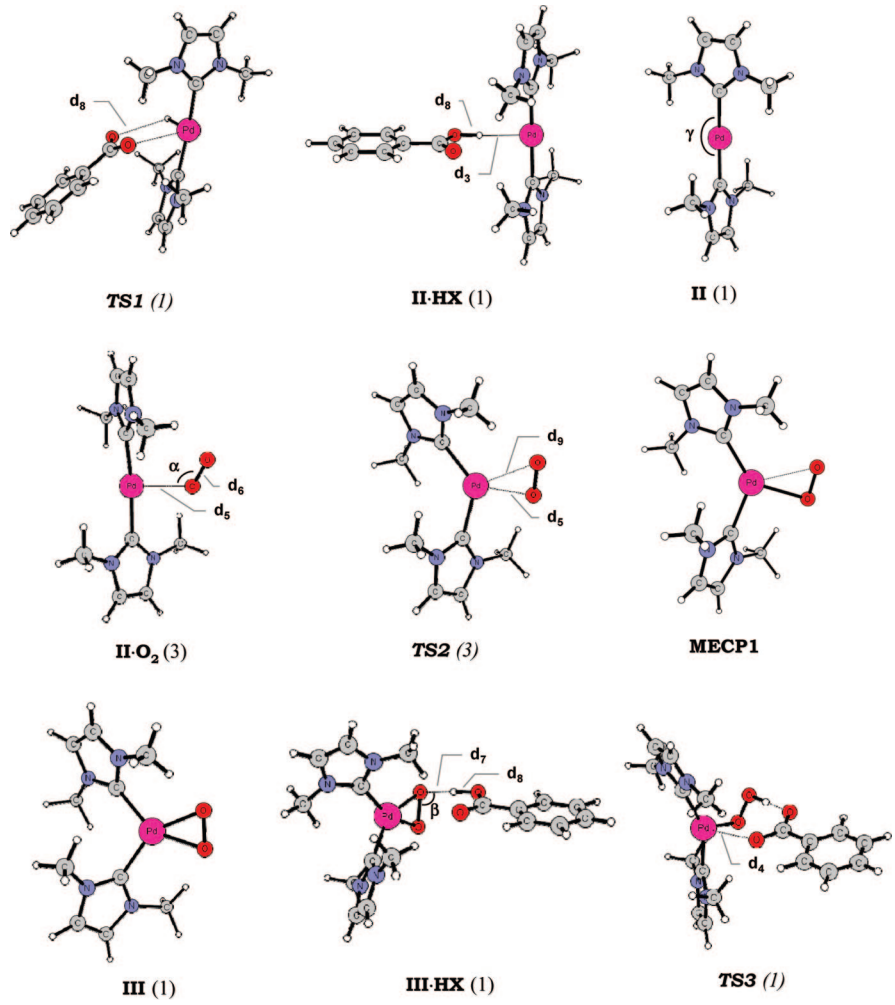

Figure 5. Ground-state optimized structures of stationary points and MECP intercepted along *Path A* in the case of R=Ph. Labels employed to individuate geometrical parameters have to be used to read information reported in Tables 1 and 2.

similar to **TS2**(3). Crossing point relative energy calculated in gas phase is reported in Figure 1. The third and final step (Step **III**→**IV**) of the examined pathway involves protonolysis of the Pd−O bond of the η^2-peroxo complex **III**. Computational analysis shows that initially CH_3COOH weakly interacts with **III** to give a hydrogen-bonded complex, **III**·HX, stabilized by 4 kcal/mol in solvent (9.6 kcal/mol in gas phase) with respect to ground-state reactants asymptote. Formation of the final hydroperoxide complex **IV** takes place overcoming an energy barrier of 23.6 and 21.2 kcal/mol in solvent and in gas phase, respectively, corresponding to the **TS3**(1) transition state. The normal mode associated with the imaginary frequency, calculated to be 161*i* cm^{-1}, corresponds to the concerted *cis* to *trans* isomerization of the IMe ligands, proton transfer from acetic acid to one of the oxygen atoms of the peroxide, and coordination of the formed acetate to the Pd center. As a result, the final singlet hydroperoxide product (CH_3CO_2)-$(IMe)_2$Pd-OOH in its *trans* configuration is obtained, and the overall process is calculated to be exothermic by 8.0 kcal/mol in benzene solvent and 17.1 kcal/mol in gas phase.

3.2. Mechanism of Direct Dioxygen Insertion into the Pd−H Bond of *trans*-[$(CH_3COO)(IMe)_2$Pd(H)]. Along the triplet pathway (see *Path B* Figure 1) the interaction of oxygen with the *trans*[$(IMe)_2(CH_3COO)$Pd−H] complex leads to the formation of a weakly bound van der Waals complex, **I**·$\mathbf{O_2}$(3), that is stabilized by about 1 kcal/mol in solution. The fully optimized structure of the corresponding complex in a singlet state is substantially different as O_2 coordinates directly to the Pd(II) center. The formed adduct, **I**·$\mathbf{O_2}$(1), is not stable and lies about 21 kcal/mol above the entrance channel of separated reactants in gas phase and 32.6 kcal/mol above, when solvation effects are included. The reported energy for this complex has been properly corrected, following the mentioned scheme,[30] since unrestricted calculations on this adduct showed a significant amount of triplet spin contamination.

The next step of the reaction, that results to be the rate-determining one, involves the abstraction of the hydrogen atom from the palladium center by O_2. This step requires an activation energy of 15.6 kcal/mol in solution and 22.9 kcal/mol in gas phase for the formation of the **TS4***(3)* transition state. In going from the first adduct to **TS4**(3) the Pd−H bond distance stretches from 1.565 to 1.763 Å, and at the same time the O−O bond length increases from 1.205 to 1.278 Å. The O−H distance is 1.237 Å indicating that the bond between oxygen and hydrogen is forming. The imaginary frequency for **TS4***(3)* transition state is calculated to be 1516*i* cm^{-1} and clearly corresponds to the movement of the hydrogen atom detaching from Pd and bonding to O

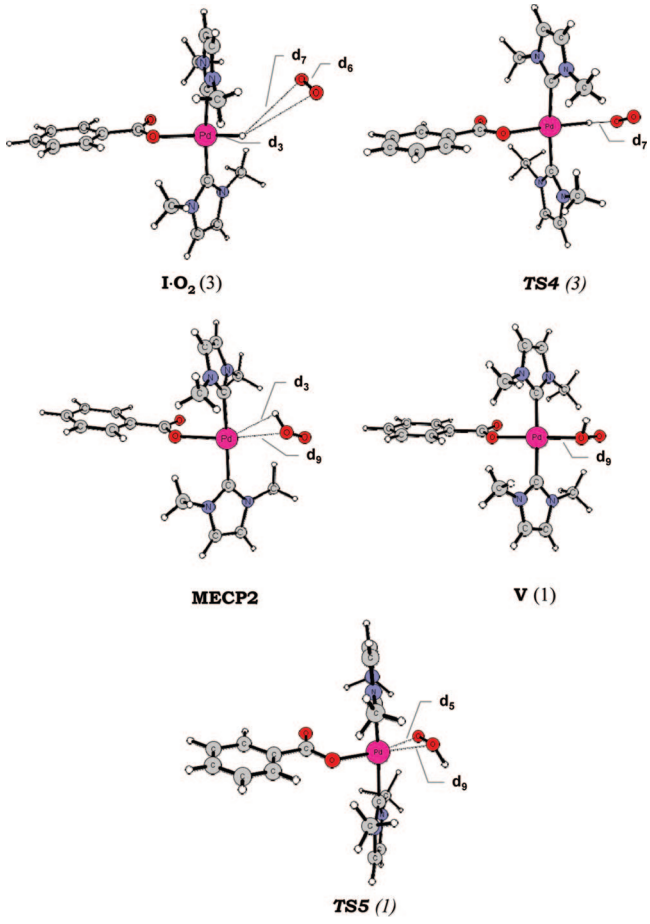

Figure 6. Ground-state optimized structures of stationary points and MECP intercepted along *Path B* in the case of R=Ph. Labels employed to individuate geometrical parameters have to be used to read information reported in Table 2.

atom. As a result, an intermediate is formed in which a peroxyl HOO radical is coordinated to the T-shaped Pd(I) complex through a weak interaction between hydrogen and Pd atoms. Indeed, this intermediate is only slightly more stable than **TS4***(3)* both in gas phase and solution. Along the singlet surface, instead, once molecular oxygen approaches the Pd center, at a distance of 1.472 Å between the closest oxygen and hydrogen, a transition state, **TS4***(1)*, has been intercepted and characterized. Also for this singlet transition state, which is less stable than the separate reactants by 35.4 kcal/mol in solution (28.4 kcal/mol in gas phase), the energy has been corrected for spin contamination. From **TS4***(1)* the reaction proceeds to yield a stable singlet intermediate, **V**(1), whose formation is endothermic by 2.9 kcal/mol in gas phase and 10.3 kcal/mol in benzene. The main feature of this intermediate is that the hydrogen atom is bonded (H−O=0.963 Å) to the proximal oxygen. Until now the existence of this kind of intermediates has not been evidenced by previous theoretical investigations.[16,19] IRC calculations confirmed that the **TS4***(1)* transition state is connected to both reactant **I·O$_2$**(3) and product **IV**(1). The analysis of the structures along the reaction coordinate from the transition state to the **IV**(1) intermediate shows that the hydrogen atom approaches the proximal oxygen lengthening the O−O bond, whereas the distal oxygen atom rotates upward.

Since the singlet state of the **IV**(1) intermediate is more stable than the triplet one, in this region of the PES the system undergoes a spin inversion that takes place after passage of the **TS4***(3)* transition state. Also in this case the spin crossover occurs after formation of the transition state and, as a consequence, cannot be considered a rate-limiting factor.[35] Relative energy calculated in gas phase of the minimum energy crossing point, **MECP2**, is reported in Figure 1. The crossing occurs in the vicinity of the triplet transition state, and the **MECP2** structure lies very close in energy to the preceding transition state. It is worthwhile to underline that all the attempts to individuate a singlet intermediate with a structure analogous to that of the triplet complex were unsuccessful in spite of the numerous strategies used to find it out.

Formation of the final hydroperoxo palladium(II) complex, along the singlet pathway involves breaking the bond between the proximal oxygen and the Pd center that makes a new bond with the distal oxygen. Triplet hydroperoxide product formation involves, instead, rearrangement of the HOO fragment in such a way that terminal oxygen and hydrogen atoms move in opposite directions toward and away from the Pd center, respectively. Both the corresponding transition states, **TS5***(1)* and **TS5***(3)*, have been intercepted and confirmed by IRC analysis. The singlet **TS5***(1)* structure lies 10.5 kcal/mol, 20.5 kcal/mol when solvent effects are included, above the reactants dissociation limit and is characterized by an imaginary frequency of 339*i* cm^{-1}. Along the triplet PES the **TS5***(3)* structure is destabilized respect to reactants by 19.6 kcal/mol in gas phase and by 28.9 kcal/mol in benzene, and the corresponding imaginary frequency is calculated to be 102*i* cm^{-1}.

Compared to the exothermic formation of the hydroperoxide product in its singlet multiplicity, **IV**(1), the overall conversion process of the palladium hydride to the Pd-OOH species, **IV**(3), along the spin conserving triplet surface is endothermic by 17.4 kcal/mol in gas phase and 24.3 kcal/mol in solvent.

3.3. Overall Mechanism for the RCO$_2$H Reductive Elimination Pathway with R=Ph, *p*-O$_2$NC$_6$H$_4$. As it appears, at a first glance, from the comparison between the left sides of Figures 1,2, and 3 the presence of a different ligand does not introduce any significant qualitative change in the calculated energy profiles. We briefly comment the quantitative description of the envisaged multistep mechanism focusing our attention on those changes that could have an influence on the determination of the most likely pathway among the two proposed ones.

The first step of the process, that is reductive elimination of the carboxylic acids, involves again formation of the weak hydrogen-bonding adduct **II·HX**(1) that occurs surmounting a high free energy barrier (see Figures 2 and 3), corresponding to the ***TS1****(1)* transition state, of 34.4 kcal/mol for R=Ph and of 31.3 kcal/mol for R=*p*-O$_2$NC$_6$H$_4$. These values are very similar to that computed for the examined acetic acid and confirm that this is the rate-determining step of the whole

Table 1. Selected Geometrical Parameters of Ground-State Reactants, Products, Intermediates, MECP, and Transition States Computed along *Path A*[a]

	I(1)(exp)	TS1(1)	II·HX(1)	II(1)	II·O_2 (3)	TS2(3)	MECP1	III(1)	III·HX(1)	TS3 (1)	IV(1)
d_1	**2.052**	**2.065**	**2.053**	2.047	2.074	2.103	2.099	2.061	**2.032**	**2.227**	**2.073**
	2.045(2.016)	*2.059*	*2.052*						*2.027*	*2.218*	*2.071*
	2.053	2.059	2.053						2.025	2.215	2.071
d_2	**2.050**	**2.058**	**2.053**	2.047	2.072	2.105	2.099	2.061	**2.061**	**2.001**	**2.058**
	2.051(2.022)	*2.058*	*2.052*						*2.061*	*2.006*	*2.061*
	2.053	2.057	2.053						2.059	2.005	2.064
d_3	**1.565**	**1.510**	**2.173**	-	-	-	-	-	-	-	-
	1.563(1.540)	*1.510*	*2.154*								
	1.559	1.510	2.102								
d_4	**2.185**	**2.932**	**3.840**	-	-	-	-	-	**3.383**	**2.903**	**2.097**
	2.187(2.134)	*3.039*	*3.819*						*3.379*	*3.145*	*2.106*
	2.195	3.116	3.816						3.399	3.238	2.113
d_5	-	-	-	-	2.392	2.256	2.279	2.036	**2.009**	**1.982**	**2.030**
									2.008	*1.980*	*2.027*
									2.007	1.979	2.016
d_6	-	-	-	-	1.259	1.284	1.305	1.400	**1.418**	**1.373**	**1.454**
									1.420	*1.371*	*1.452*
									1.422	1.374	0.967
d_7	-	-	-	-	-	-	-	-	**1.551**	**1.067**	**0.966**
									1.498	*1.048*	*0.966*
									1.424	1.035	1.452
d_8	-	**2.414**	**1.000**						**1.031**	**1.435**	-
	-	*2.517*	*1.014*	-	-	-	-	-	*1.046*	*1.479*	
		2.578	1.024						1.074	1.514	
d_9					3.218	2.572	2.312	2.036	**2.084**	**2.539**	-
	-	-	-	-					*2.089*	*2.574*	
									2.097	2.579	
α					120.5	88.8	74.8	69.9	**72.6**	**96.7**	**113.4**
	-	-	-	-					*72.9*	*98.7*	*113.5*
									76.2	99.0	101.3
β				-	-	-	-	-	**104.0**	**96.7**	**101.2**
	-	-	-						*97.9*	*103.7*	*101.3*
									102.6	103.5	113.7
γ	**175.9**	**175.1**	**178.5**	179.9	174.6	127.2	119.8	105.8	**100.8**	**140.5**	**177.6**
	175.3	*175.1*	*179.2*						*100.2*	*150.8*	*177.2*
	174.5	174.8	178.7						99.8	150.6	177.4
θ	**48.6**	**−71.1**	**0.0**	-	-	-	-	-	-	-	-
	10.9	*−67.4*	*0.0*								
	0.3	−69.7	0.0								

[a] Available experimental geometrical parameters for the benzoate analogue of the hydride complex are also reported in parentheses.Values are reported in **bold** for R=CH_3, in *italic* for R=Ph, and in regular for *p*-$O_2NC_6H_4CO_2$. Bond lengths are in Å and angles are in degrees. θ = N−C−C−N dihedral angle to individuate relative positions of IMe ligands.

oxygenation pathway. Formation of the Pd(0) complex is more endothermic for both R=Ph and R=*p*-$O_2NC_6H_4$ with respect to the elimination of acetic acid as well as, consequently, formation of the subsequent two minima and transition state since the $(IMe)_2Pd(0)$ oxygenation step does not depend on the employed carboxylic acid. Identical is also the structure of the minimum energy crossing point, **MECP1**, between the triplet and singlet surfaces.

The interaction of the carboxylic acid RCOOH with the η^2-peroxo complex **III**(1) is exothermic in solvent by −6.8 and −3.3 kcal/mol with respect to ground-state reactants asymptote for R=Ph and *p*-$O_2NC_6H_4$, respectively. The free energy barrier that is necessary to surmount to obtain the final hydroperoxide product **IV** is 14.6 kcal/mol for R=Ph and 10.5 kcal/mol for R=*p*-$O_2NC_6H_4$. Proton transfer from the carboxylic acid to one of the oxygen atoms of the peroxide, coordination of the formed anion to the Pd center, and *cis* to *trans* isomerization of the IMe ligands allow formation of the final singlet hydroperoxide complex (RCO_2)-$(IMe)_2$Pd-OOH in its *trans* configuration. The overall process is calculated to be exothermic by about 8 kcal/mol in benzene solvent for both R=Ph and *p*-$O_2NC_6H_4$, being that this value is very close to that calculated in the case of the reductive elimination of acetic acid.

3.4. Mechanism of Direct Dioxygen Insertion into the Pd−H Bond of *trans*-[RCOO(IMe)$_2$Pd(H)] with R=Ph and *p*-$O_2NC_6H_4$. As it was pointed out yet in the previous paragraph, no significant qualitative differences emerge between the calculated energy profiles when the right sides of Figures 1, 2, and 3 are compared. However, it is worth highlighting some quantitative differences. The interaction of triplet oxygen with the *trans*-$[(RCO_2)(IMe)_2PdH]$ complex leads to the formation of a weakly bound van der Waals complex, **II·HX**(1), that is endothermic in solvent by about 7 kcal/mol both for R=Ph and R=*p*-$O_2NC_6H_4$ and more endothermic than R=CH_3. Along the triplet surface the reaction evolves through the abstraction of the hydrogen atom from the palladium center by O_2. This step takes place overcoming a free energy barrier of 24.8 and 22.7 kcal/mol for R=Ph and R=*p*-$O_2NC_6H_4$, respectively, corresponding to the formation of the ***TS4(3)*** transition states. The imaginary frequencies that confirm the nature of these stationary points correspond to the shift of the hydrogen atom from Pd to one of the O atoms. The intermediate **V**(3) that is formed can be again classified as an adduct in which the peroxyl HOO radical is coordinated to the T-shaped Pd(I) complex through a weak interaction between hydrogen and Pd atoms. Indeed, this reaction intermediate lies just a few

Table 2. Selected Geometrical Parameters of Ground-State Intermediates, MECP, and Transition States Computed along *Path B*[a]

	I·O$_2$ (3)	**TS4(3)**	**MECP2**	**V(1)**	**TS5(1)**
	2.051	**2.063**	**2.093**	**2.075**	**2.074**
d$_1$	*2.052*	*2.064*	*2.091*	*2.073*	*2.073*
	2.052	2.066	2.092	2.074	2.072
	2.049	**2.063**	**2.082**	**2.066**	**2.042**
d$_2$	*2.049*	*2.062*	*2.106*	*2.064*	*2.042*
	2.051	2.062	2.108	2.066	2.044
	1.565	**1.762**	**2.452**		
d$_3$	*1.562*	*1.764*	*2.455*	-	-
	1.559	1.764	2.457		
	2.186	**2.220**	**2.226**	**2.070**	**2.066**
d$_4$	*2.191*	*2.218*	*2.263*	*2.076*	*2.069*
	2.199	2.227	2.284	2.082	2.075
	4.662	**3.679**	**3.449**	**2.999**	**2.478**
d$_5$	*4.573*	*3.649*	*3.444*	*3.000*	*2.476*
	4.548	3.646	3.441	2.990	2.468
	1.205	**1.277**	**1.352**	**1.481**	**1.517**
d$_6$	*1.205*	*1.277*	*1.351*	*1.479*	*1.518*
	3.466	1.235	1.348	0.964	0.965
	3.386	**1.237**	**0.984**	**0.963**	**0.965**
d$_7$	*3.488*	*1.239*	*0.983*	*0.963*	*0.965*
	1.205	1.276	0.983	1.478	1.519
			2.735	**2.086**	**2.258**
d$_9$	-	-	*2.737*	*2.088*	*2.251*
			2.731	2.083	2.243
			48.0	**39.7**	**63.5**
α	-	-	*47.7*	*39.7*	*63.4*
			47.8	39.8	63.3
		111.1	**106.7**	**101.8**	**101.8**
β	-	*111.2*	*106.5*	*101.7*	*101.7*
		111.2	106.7	101.8	101.7
	176.1	**174.4**	**177.7**	**177.2**	**176.9**
γ	*175.8*	*175.2*	*178.3*	*177.6*	*177*
	175.3	174.7	178.2	178.0	177.5
	47.8	**48.2**	**17.4**	**6.4**	**10.2**
θ	*49.2*	*8.1*	*26.9*	*7.1*	*9.7*
	49.7	2.1	27.4	6.7	8.1

[a] Values are reported in **bold** for R=CH_3, in *italic* for R=Ph, and in regular for *p*-$O_2NC_6H_4CO_2$. Bond lengths are in Å and angles are in degrees. θ = N−C−C−N dihedral angle to individuate relative positions of IMe ligands.

kcal/mol below the ***TS4(3)*** transition state for both $PhCO_2$ and *p*-$O_2NC_6H_4CO_2$ ligands.

Along the singlet surface, instead, overcoming the energy barrier for the intercepted transition state, **TS4***(1)*, allows the formation of a singlet intermediate, **V**(1), whose main feature is that the hydrogen atom is bonded to the proximal oxygen. Also in this case IRC calculations confirmed that the ***TS4(1)*** transition states are connected to both reactant **II·O$_2$**(1) and product **V**(1). Formation of the singlet intermediate **V**(1) is more favorable with respect to formation of the corresponding triplet intermediate by about 10 kcal/mol in solvent, as for R=CH_3. This means that the system must undergo a spin inversion that takes place after passage of the **TS4**(3) transition state. Geometrical parameters of the computed structures of the minimum energy crossing points, **MECP2**, between the triplet and singlet surfaces, are reported in Table 2, and their relative energies calculated in gas phase are reported in Figures 2 and 3 for R=Ph and R=*p*-$O_2NC_6H_4$, respectively.

Formation of the final palladium(II) hydroperoxo product takes place, along the singlet pathway, through the **TS5***(1)* transition state that lies 19.7 kcal/mol for R=Ph and 21.6 kcal/mol for R=*p*-$O_2NC_6H_4$ above the ground-state reactants asymptote. Rearrangement of the HOO fragment, instead, allows triplet hydroperoxide product formation through the corresponding less stable, for both benzoate and *p*-nitrobenzoate ligands, **TS5***(3)* transition states. Energetics of the hydroperoxide product reaction formation along both singlet and spin conserving triplet surfaces have been reported in the preceding paragraph.

3.5. Preferred Mechanism and Ligand Influence. The detailed and systematic analysis of the two viable palladium-hydride oxygenation pathways carried out in this work reveals that the free activation energies for the rate determining-step of *Path A* and *Path B* are different enough, in spite of the intrinsic uncertainties of DFT computations, to determine which is the preferred mechanism. When the involved carboxylic acid is the acetic acid, the calculated barrier for the CH_3COOH reductive elimination initial step (*Path A*) is 31.2 kcal/mol in gas phase and 31.0 kcal/mol when salvation effects are included. The rate-determining step barrier that is necessary to overcome, instead, for the abstraction of the hydrogen atom by molecular oxygen (*Path B*) is 15.6 and 22.9 kcal/mol in gas phase and in benzene, respectively. The two examined mechanisms exhibit the same difference in the calculated activation barriers relative to the rate-determining step even when the ligands coordinated to the Pd center of the initial Pd-hydride complex are $PhCO_2$ and *p*-$O_2NC_6H_4CO_2$. Indeed, free activation energies calculated in solvent are 34.4 and 24.8 kcal/mol for the reductive elimination and hydrogen atom abstraction steps, respectively when R=Ph. Analogous barriers are 31.3 and 22.7 kcal/mol when R=*p*-$O_2NC_6H_4$. Therefore, on the basis of our results the oxygenation reaction is more likely to evolve through direct insertion of molecular oxygen into the Pd−H bond of the initial hydride complex. This conclusion is reinforced by the favorable comparison between the experimental activation energy, determined to be 24.4(5) kcal/mol for the benzoate ligand,[18] and the corresponding calculated value of 24.8 kcal/mol. In addition, the experimentally detected enhancement of the oxygenation rate due to the presence of the nitro group on the benzoate ligand corresponds to the lower activation energy calculated by us for R=*p*-$O_2NC_6H_4$.

Conclusions

A detailed DFT study of the mechanism for the conversion of the Pd(II)-hydride complex, $(IMe)_2(RCO_2)PdH$ (R=CH_3, Ph, and *p*-$O_2NC_6H_4$), to the corresponding Pd(II)-hydroperoxide in the presence of molecular oxygen has been carried out with the aim to probe the alternative reaction pathways, both considered viable on the basis of current data, of direct O_2 insertion, and slow reductive elimination followed by oxygenation. The outcome of our computational analysis supports the mechanism of direct insertion of molecular oxygen into the Pd−H bond of the initial complex. The activation energy relative to the rate-determining step of the direct insertion pathway is calculated to be lower than the activation energy of the rate determining step of the alternative pathway that

involves the carboxylic acid reductive elimination, whatever ligand (CH_3CO_2, Ph, CO_2, p-$O_2NC_6H_4CO_2$) is coordinated to the Pd center. The calculated free activation energy of the rate-determining hydrogen abstraction step ($\Delta G^* = 24.8$ kcal/mol) in the case of the oxygenation reaction of the benzoate-ligated Pd(II)-hydride complex is in very good agreement with the value experimentally determined ($\Delta G^* = 24.4$ kcal/mol). In addition, according to the experimentally detected enhancement of the reaction rate due to the presence of the nitro group on the benzoate ligand, our calculations show that the transition state for the hydrogen atom abstraction by molecular oxygen lies lower in energy along the pathway for the oxygenation reaction of $(IMe)_2(p\text{-}O_2NC_6H_4CO_2)PdH$.

Acknowledgment. We gratefully acknowledge financial help from the Università della Calabria.

References

(1) Stahl, S. S. *Science* **2005**, *309*, 1824–1826.

(2) Stahl, S. S. *Angew. Chem., Int. Ed.* **2004**, *43*, 3400–3420.

(3) Sigman, M. S.; Schultz, M. J. *Org. Biomol. Chem.* **2004**, *2*, 2551–2554.

(4) Stoltz, B. M. *Chem. Lett.* **2004**, *33*, 362–367.

(5) Nishimura, T.; Uemura, S. *Synlett* **2004**, 201–216.

(6) Sheldon, R. A.; Arends, I. W. C. E.; ten Brink, G.-J.; Dijksman, A. *Acc. Chem. Res.* **2002**, *35*, 774–781.

(7) Gligorich, K. M.; Sigman, M. S. *Angew. Chem., Int. Ed.* **2006**, *45*, 6612–6615.

(8) Konnick, M. M.; Guzei, I. A.; Stahl, S. S. *J. Am. Chem. Soc.* **2004**, *126*, 10212–10213.

(9) Stahl, S. S.; Thorman, J. L.; Nelson, R. C.; Kozee, M. A. *J. Am. Chem. Soc.* **2001**, *123*, 7188–7189.

(10) Thiel, W. R. *Angew. Chem.* **1999**, *111*, 3349–3351. *Angew. Chem., Int. Ed.* **1999**, *38*, 3157−3158.

(11) Nishimura, T.; Onoue, T.; Ohe, K.; Uemura, S. *J. Org. Chem.* **1999**, *64*, 6750–6755.

(12) Hosokawa, T.; Murahashi, S.-I. *Acc. Chem. Res.* **1990**, *23*, 49–54.

(13) Muzart, J.; Pete, J. P. *J. Mol. Catal.* **1982**, *15*, 373–376.

(14) Landis, C. R.; Morales, C. M.; Stahl, S. S. *J. Am. Chem. Soc.* **2004**, *126*, 16302–16303.

(15) Denney, M. C.; Smythe, N. A.; Cetto, K. L.; Kemp, R. A.; Goldberg, K. I. *J. Am. Chem. Soc.* **2006**, *128*, 2508–2509.

(16) Keith, J. M.; Muller, R. P.; Kemp, R. A.; Goldberg, K. I.; Goddard, W. A., III; Oxgaard, J. *Inorg. Chem.* **2006**, *45*, 9631–9633.

(17) Keith, J. M.; Nielsen, R. J.; Oxgaard, J.; Goddard, W. A., III *J. Am. Chem. Soc.* **2005**, *127*, 13172–13179.

(18) Konnick, M. M.; Gandhi, B. A.; Guzei, I. A.; Stahl, S. S. *Angew. Chem., Int. Ed.* **2006**, *45*, 2904–2907.

(19) Popp, B. V.; Stahl, S. S. *J. Am. Chem. Soc.* **2007**, *129*, 4410–4422.

(20) Chowdhury, S.; Rivalta, I.; Russo, N.; Sicilia, E. *Chem. Phys. Lett.* **2007**, *443*, 183–189.

(21) Chowdhury, S.; Rivalta, I.; Russo, N.; Sicilia, E. *Chem. Phys. Lett.* **2008**, *456*, 41–46.

(22) Gligorich, K. M.; Sigman, M. *Angew. Chem., Int. Ed.* **2006**, *45*, 6612–6615.

(23) Becke, A. D. *J. Chem. Phys.* **1993**, *98*, 5648–5652.

(24) Stephens, P. J.; Devlin, F. J.; Chabalowski, C. F.; Frisch, M. J. *J. Phys. Chem.* **1994**, *98*, 11623–11627.

(25) Frisch, M. J.; Trucks, G. W.; Schlegel, H. B.; Scuseria, G. E.; Robb, M. A.; Cheeseman, J. R. ; Montgomery, J. A., Jr.; Vreven, T.; Kudin, K. N. ; Burant, J. C.; Millam, J. M.; Scalmani, G.; Rega, N.; Petersson, G. A.; Nakatsuji, H.; Hada, M.; Ehara, M.; Toyota, K.; Fukuda, R.; Hasegawa, J.; Ishida, M.; Nakajima, T.; Honda, Y.; Kitao, O.; Nakai, H.; Klene, M.; Li, X.; Knox, J. E.; Hratchian, H. P.; Cross, J. B.; Bakken, V.; Adamo, C.; Jaramillo, J.; Gomperts, R.; Stratmann, R. E.; Yazyev, O.; Austin, A. J.; Cammi, R.; Pomelli, C.; Ochtersky, ; Ayala, P. Y.; Morokuma, ; Voth, ; Salvador, ; Dannenberg, ; Zakrzewski, ; Dapprich, ; Daniels, ; Strain, ; Farkas, ; Malick, ; Rabuck, ; Raghavachari, ; Foresman, ; Ortiz, ; Cui, ; Baboul, ; Clifford, ; Cioslowski, ; Stefanov, ; Liu, ; Liashenko, ; Piskorz, ; Komaromi, ; Martin, ; Fox, ; Keith, ; Al-Laham, ; Peng, ; Nanayakkara, ; Challacombe, ; Gill, ; Johnson, ; Chen, ; Wong, ; Gonzalez, ; Pople, *Gaussian03, reVision B.05*; Gaussian, Inc.: Wallingford, CT, 2004.

(26) Andrae, D.; Häussermann, U.; Dolg, M.; Stoll, H.; Preuss, H. *Theor. Chim. Acta* **1990**, *77*, 123–141.

(27) Fukui, K. *J. Phys. Chem.* **1970**, *74*, 4161–4163.

(28) Gonzalez, C.; Schlegel, H. B. *J. Chem. Phys.* **1989**, *90*, 2154–2161.

(29) Weissbluth, M. *Atoms and Molecules*; Academic Press: New York, 1978; p 587.

(30) Ovchinnicov, A. A.; Labanowski, J. K. *Phys. Rev. A* **1996**, *53*, 3946–3952.

(31) Cancès, M.; Mennucci, B.; Tomasi, J. *J. Chem. Phys.* **1997**, *107*, 3032–3041.

(32) Mennucci, B.; Cancès, E.; Tomasi, J. *J. Phys. Chem. B* **1997**, *101*, 10506–10507.

(33) Kollaman, P. *Chem. Rev.* **1993**, *93*, 2395.

(34) Harvey, J. N.; Aschi, M.; Schwarz, H.; Koch, W. *Theor. Chem. Acc.* **1998**, *99*, 95–99.

(35) Cramer, C. J.; Tolman, W. B.; Theopold, K. H.; Rheingold, A. L. *PNAS* **2003**, *100*, 3635–3640.

(36) Schröder, D.; Shaik, S.; Schwarz, H. *Acc. Chem. Res.* **2000**, *33*, 139–145.

CT8001442